

Effect of low-frequency AC forcing on the morphological instability arising in electrodeposition

Akash Ganesh · Dipin S. Pillai · R. Narayanan

Received: 8 August 2021 / Accepted: 20 November 2021 / Published online: 31 December 2021 © The Author(s), under exclusive licence to Springer Nature B.V. 2021

Abstract Electrodeposition in the presence of a DC field is an unstable process leading to morphological patterns on the cathode. The effect of a low-frequency and small amplitude AC forcing superimposed on a base DC field, ΔV , is investigated by perturbation theory and Floquet analysis. It is shown that we can forecast the stability behavior of the AC problem from the nature of the graph of electrode base speed, U, versus ΔV . The key finding is this: when this graph is always of negative curvature, the effect of AC forcing is stabilizing, whereas when the curvature changes sign, the effect of AC forcing can be either destabilizing or stabilizing. The difference in the two types of $U-\Delta V$ curves is characterized by a single dimensionless group that signals the change from diffusion-controlled transport to transport controlled by reaction kinetics at the electrodes. The critical value of this parameter that marks the transition is obtained analytically.

Keywords Electrodeposition · Linear stability · Morphological instability · Periodic field

Mathematics Subject Classification 00A69 · 00A79 · 76E17 · 7010

1 Introduction

Electrodeposition of metal occurs when an electrical potential is imposed across two flat metal surfaces separated by an ionic solution. In a typical electrodeposition process, the metal with the higher potential, the anode, is where metallic oxidation is predominant, while the second metal which is at the lower potential, the cathode, is where metallic reduction is predominant. The potential difference is imposed by applying a finite voltage between the electrodes. The planar electrode surfaces that participate in the process can become wavy due to an interfacial

A. Ganesh · R. Narayanan

Department of Chemical Engineering, University of Florida, Gainesville, FL 32611, USA

e-mail: akash.ganesh@ufl.edu

R. Narayanan

e-mail: ranga@ufl.edu

D. S. Pillai (⊠)

Department of Chemical Engineering, Indian Institute of Technology Kanpur, Kanpur, Uttar Pradesh 208016, India e-mail: dipinsp@iitk.ac.in



16 Page 2 of 18 A. Ganesh et al.

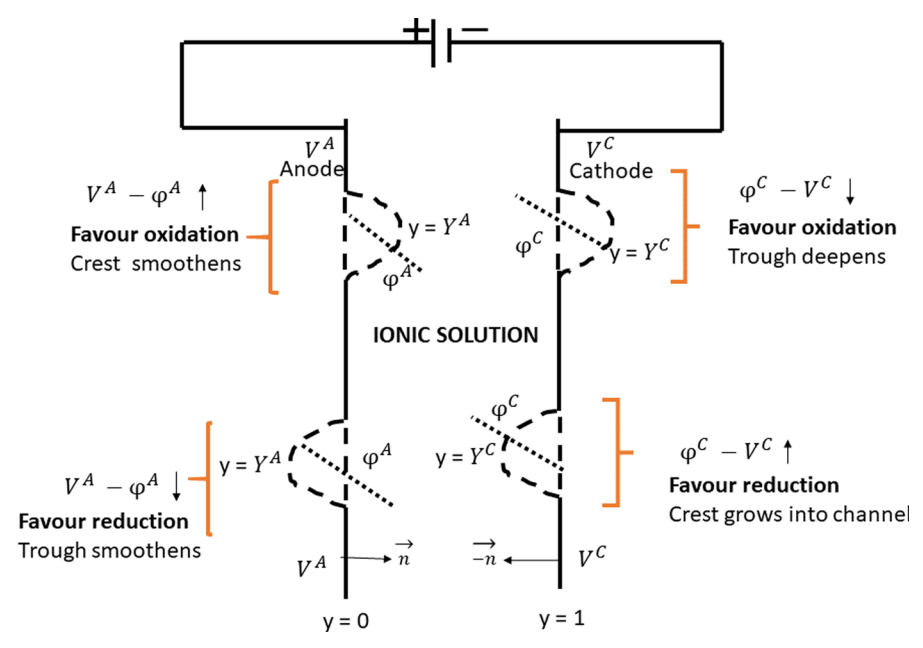


Fig. 1 Physics of morphological instability associated with electrodes during electrodeposition. The heavy dashed curves are the perturbations to electrode surfaces and the dotted line represents the extrapolation of the base potential profile into the solution. The vector, **n**, is the unit normal pointing into the solution. In the base state, both planar electrodes move toward the left with a speed, *U*

instability [1–5]. Several studies on the evolution of the morphology of electrode surfaces and the factors that determine the growth rate of wavy patterns have been carried out in the past [6–11].

The instability that occurs in electrodeposition, i.e., the growth of wavy patterns consisting of selected wavelengths at the electrode surface is due to a trade-off between stabilizing and destabilizing effects. To see why this is so, consider the schematic presented in Fig. 1. A specific example of copper electrodes separated by a dilute copper sulfate electrolytic solution is taken. At the anode, which is at a higher potential, V^A , copper metal is oxidized releasing cupric ions which transport through the solution via a concentration gradient and a potential gradient. At the cathode, which is at a lower potential, V^{C} , the cupric ions undergo reduction to metallic copper. As the figure depicts, any arbitrary displacement of the cathode surface into the solution increases the potential difference between the solution and the electrode, $\phi^C - V^C$, thereby enhancing the charge transfer rate and reinforcing the rate of metal deposition. This effect is destabilizing and is independent of the wavenumber of the displacement, denoted k. The opposite phenomenon occurs at the anode. The destabilizing effects are countered by the stabilizing effect offered by the curvature of the surface, which increases the energy of activation of the electrochemical reaction, hence weakening the rate of metal deposition at a crest. This stabilizing effect of curvature, however, is k dependent [11]. In other words, the wavelength selection in electrodeposition owes its origins to the surface energy of the metal in the presence of the electrolytic solution. While the explanation given above refers to the crests depicted in Fig. 1, a similar one can be given for the troughs, also depicted in the same figure [2,11]. It might be noted that the physical explanation given above for electrodeposition instability has analogs in many other interfacial instability problems such as solidification, evaporation, and viscous fingering [12–16].

Denoting the linear growth rate of a disturbance by σ , several theories have been developed for σ vs k^2 curves [6–9,11,17–19]. A typical σ vs k^2 curve in electrodeposition initially increases, reaches a maximum, and then decreases, crossing zero at a critical value of k^2 called the neutral point. Beyond the neutral point, disturbances of all wavenumbers are stable with their corresponding growth rates, σ , being negative. Past workers [8,11] developed a two-electrode model for obtaining the σ vs k^2 curves by expressing the governing equations in the domain, i.e., the electrolyte solution and the boundaries, i.e., the electrode surfaces, as a function of three input variables, viz., the average metal ion concentration, the spacing between the electrodes, and the input voltage difference applied across the electrodes. One of the objectives of their studies was to see the effect on the neutral point of these input variables.



Fig. 2 An overview of the theoretical analysis. The objective is to determine the effect of AC of a small amplitude, δ , in addition to a base DC. This is carried out as a double perturbation series. A linear stability analysis is carried out in the form of series expansion in ϵ . For both cases of steady flat electrodes $(\mathcal{O}(\epsilon^0))$ and deflected electrodes $(\mathcal{O}(\epsilon))$, the problem is further expanded in regular perturbation series in δ to determine the influence of AC

The models that were developed earlier pertained to the case of constant applied DC voltage [6–11]. Inspired by the physics of stabilizing erstwhile unstable systems with periodic forcing, observed in a vast number of examples [20–22], one is encouraged to investigate the effect of AC forcing on electrodeposition. Therefore, the goal of the current work is to determine the effect of an addition of a small AC forcing, of the form $\delta \cos(\Omega t)$, to a constant DC voltage on the σ vs k^2 curve. Here, δ is the amplitude of the small AC forcing of frequency, Ω , and t denotes time. In particular, a shift of the neutral point toward higher wavenumber indicates a destabilizing effect, while a shift toward lower wavenumber indicates a stabilizing effect. Our analysis will show that the effect of the small AC voltage on a base DC can first be seen only at $\mathcal{O}\left(\delta^2\right)$ and that it arises from the time-independent component at that order due to the effect of AC voltage appearing as $\cos^2(\Omega t)$. This in turn is $1/2 + 1/2\cos(2\Omega t)$, i.e., a sum of a pseudo-DC component and a time-dependent component.

An overview of our theoretical analysis is presented in Fig. 2. Unlike periodic forcing in hydrodynamic instability problems [20–22], this study will show that a small AC forcing on a DC problem may lead either to further destabilization or stabilization, depending on the electrode spacing and the base-applied DC voltage, characterized principally by two non-dimensional groups. The results of this study hint toward the practical possibility of either completely suppressing the instability or obtaining well-defined patterns on the electrode surface.

We first present the nonlinear modeling equations in dimensionless form along with their physical interpretation and the assumptions that are made in deriving the model. The validity and consequences of the assumptions that are made to simplify the equations are also discussed. We then perform a linear stability analysis by perturbing the variables about a steady-state solution, i.e., the base state, to obtain the growth rate, σ , of a displacement of a wave number, k. In general, the problem with AC forcing leads to a set of complicated interdependent equations, wherein an explicit relationship between σ and k^2 is not obtained. The equations are, therefore, solved computationally using Floquet theory [23,24].

2 The theoretical model

2.1 The nonlinear equations

The theoretical model presented hereunder is developed upon the lines presented by BuAli et al. [11]. The nonlinear equations describing the concentration and potential profiles in the electrolyte solution, as well as the metal–solution



16 Page 4 of 18 A. Ganesh et al.

interface of both electrodes in terms of scaled variables are presented. The analysis is conveniently performed when the observer is situated on the moving frame of the erstwhile flat electrode. Figure 1 depicts the coordinate system in a moving frame with the observer situated on the moving electrode in the base planar state. The change in frame involves the base speed of the electrode surface in the laboratory frame. This base speed is scaled by its limiting value, U_{lim} , where $U_{\text{lim}} = \frac{2c_{\text{ref}}[z_1-z_2]D_1}{z_1z_2c_ML}$. The velocity of the perturbed electrode surface in the moving frame is, however, scaled by $\frac{D}{L}$, where D is given by $\frac{[z_1-z_2]D_1D_2}{z_1D_1-z_2D_2}$. Here, L is the electrode spacing, c_{ref} is the average metal ion concentration, and D_1 and D_2 are the diffusion coefficients of the ionic species of valence z_1 and z_2 , for example, the cupric and sulfate ions in a copper sulfate solution. All lengths are scaled by the electrode spacing, L. This is because the electrode spacing in our model is smaller than the maximum concentration boundary layer thickness, given by D/U_{lim} . The ion concentration is scaled by c_{ref} , the electrical potential by $\frac{RT}{z_1F}$, and time by $\frac{L^2}{D}$. The symbols, T and F, stand for the absolute temperature and Faraday constant, respectively.

The equations in the electrolytic solution are developed from the transport equations, i.e., the conservation laws of the two ionic species, while the equations at the metal-solution interfaces are developed from the mass balance of the species at the interfaces using four standard assumptions [2]. These are local electrical neutrality in the solution, diluteness of the ionic species, fixed volume of the electrolyte solution, and negligible convective effects. These assumptions have been justified in several studies of electrodeposition [1,8,11]. With the above scalings, the nonlinear equations become

$$\frac{\partial c}{\partial t} = \nabla^2 c \quad \text{and} \quad \mathcal{P}\nabla^2 c + \nabla \cdot (c\nabla\phi) = 0,$$
 (1)

in the electrolyte solution, and

$$\mathbf{n} \cdot \nabla c = -2\mathbf{n} \cdot (\mathbf{U} + \mathcal{C}\mathbf{u})$$
 and $\mathbf{n} \cdot c \nabla \phi = -2\mathcal{Z}\mathbf{n} \cdot (\mathbf{U} + \mathcal{C}\mathbf{u}),$ (2)

at the metal-solution interface at both electrodes, $y = Y^A(x, t)$, i.e., the anode, and $y = 1 + Y^C(x, t)$, i.e., the cathode (cf. Fig. 1). The parameter, \mathcal{P} , is defined via

$$\mathcal{P} = \frac{z_1[D_1 - D_2]}{z_1D_1 - z_2D_2},$$

and takes the value of -3/17 for the copper–copper sulfate system.

Note that our model is taken to be 2D, i.e., in y and x, without any loss of generality. In the above, c denotes the scaled value of z_1c_1 or $-z_2c_2$, where the local electroneutrality assumption has been invoked. The speed of the electrode surfaces in the moving frame is given by $u = \mathbf{u} \cdot \mathbf{n}$ and the speed of the planar surfaces in the laboratory frame is U. Thus, in Eq. (2), $\mathbf{U} = U\mathbf{j}$. As a result of the volume conservation assumption, we have $\int_{Y^A}^{1+Y^C} c \, dy = 1$.

In addition to the above equations, there are two rate equations which describe the charge transfer taking place at both electrode surfaces. These rate equations are termed the Butler–Volmer equations [1] and are

$$\mathcal{B}\mathbf{n} \cdot (\mathbf{U} + \mathcal{C}\mathbf{u}) = \mathbf{e}^{[1-\beta][V^A - \phi^A - \Delta_{\text{ref}} - A2H^A]} - c^A \mathbf{e}^{-\beta[V^A - \phi^A - \Delta_{\text{ref}} - A2H^A]},\tag{3}$$

at the anode, and

$$-\mathcal{B}\mathbf{n}\cdot(\mathbf{U}+\mathcal{C}\mathbf{u}) = e^{[1-\beta][V^C - \phi^C - \Delta_{\text{ref}} - \mathcal{A}2H^C]} - c^C e^{-\beta[V^C - \phi^C - \Delta_{\text{ref}} - \mathcal{A}2H^C]},\tag{4}$$

at the cathode. The superscripts A and C denote the evaluation of the variables at the anode and the cathode, respectively, and Δ_{ref} refers to the equilibrium potential difference of the planar electrode surface in contact with



Table 1 Properties used in our computations for a pair of copper electrodes and copper-sulfate solution [11]

Property	Symbol	Value	
Molar density of copper (kg mol/m³)	c_M	150	
Surface energy density (J/m ²)	γ	1.5	
Diffusivity of copper ions (m ² /s)	D_1	7×10^{-10}	
Diffusivity of sulfate ions (m ² /s)	D_2	10^{-9}	
Exchange current density (A/m ²)	$i_{ m ref}$	10 for $c_{\text{ref}} = 0.1 \text{ kg mol/m}^3$,	
		3.2 for $c_{\text{ref}} = 0.01 \text{ kg mol/m}^3$	
Symmetry factor	$oldsymbol{eta}$	1/2	
Faraday constant (C/gmol)	F	96500	
Absolute Temperature (K)	T	298.15	

Observe that D for this system is 8.24×10^{-10}

the electrolytic solution [2]. Note that

$$\mathbf{n} \cdot \mathbf{u} = \frac{\frac{-\partial Y^C}{\partial t}}{\left[1 + \left(\frac{\partial Y^C}{\partial x}\right)^2\right]^{1/2}} \text{ at the cathode}$$

and

$$\mathbf{n} \cdot \mathbf{u} = \frac{\frac{\partial Y^A}{\partial t}}{\left[1 + \left(\frac{\partial Y^A}{\partial x}\right)^2\right]^{1/2}} \text{ at the anode.}$$

Further,

$$2H^C = \frac{\frac{-\partial^2 Y^C}{\partial x^2}}{\left[1 + \left(\frac{\partial Y^C}{\partial x}\right)^2\right]^{3/2}}$$
 at the cathode

and

$$2H^A = \frac{\frac{\partial^2 Y^A}{\partial x^2}}{\left[1 + \left(\frac{\partial Y^A}{\partial x}\right)^2\right]^{3/2}}$$
 at the anode.

Observe the scaled equations contain three non-dimensional groups, viz.:

$$\mathcal{A} = \frac{\gamma}{RTc_ML}, \quad \mathcal{B} = \frac{2Fc_{\text{ref}}D_1[1+\mathcal{Z}]}{i_{\text{ref}}L} \quad \text{and} \quad \mathcal{C} = \frac{\frac{D}{L}}{\frac{2c_{\text{ref}}[z_1-z_2]D_1}{z_1z_2c_ML}},$$

where $\mathcal{Z} = -\frac{z_1}{z_2}$, γ denotes the surface energy per unit area, i_{ref} denotes the exchange current density, obtained from the Nernst equation and, therefore, depends on c_{ref} , and c_M denotes the molar density of the metal electrode. The group $\mathcal A$ is indicative of the surface energy effects, the product $\mathcal B\mathcal C$ is the ratio of diffusive time scale to kinetic time scale, and $\mathcal C$ is the ratio of diffusive speed to the limiting speed, U_{lim} . Their orders of magnitude for a typical copper–copper sulfate solution, whose properties are given in Table 1, are presented in Table 2.



16 Page 6 of 18
A. Ganesh et al.

71							
L(m)	$c_{\rm ref}$ (kg mol/m ³)	\mathcal{A}	\mathcal{B}	С	BC		
10^{-4}	0.1	4.03×10^{-5}	27.02	-882.353	-23841.2		
8.01×10^{-4}	0.1	5.03×10^{-6}	3.3723	-882.353	-2975.56		
10^{-2}	0.1	4.03×10^{-7}	0.27	-882.353	-238.412		
10^{-4}	0.01	4.03×10^{-5}	8.44	-8823.53	-74470.6		
10^{-2}	0.01	4.03×10^{-7}	0.0844	-8823.53	-744.706		

Table 2 Typical values for the dimensionless parameters

(a) 1.2		Т		(b)	
				(2)	σ^{A} without approximation
1 -	ت من			3.00e-03	$\sigma^{\rm C}$ without approximation
		····· With a	pproximation		σ^{A} with approximation
0.8	//	Withou	it approximation -	2.00e-03	σ^{C} with approximation
□ 0.6			_	1.00e-03	1.2
0.4			_	0.00e+00	100 102 104
0.2	/		-	-1.00e-03	
0				-2.00e-03	
0	10 20	30	40	-2.00e-03	
		V			1 # #

Fig. 3 a U vs V, $\mathcal{B} = 27$. b σ vs k^2 , V = 14.2 and $\mathcal{B} = 27$ for two models: (i) the full nonlinear model given by the solid curve and (ii) the simplified model given by the dotted curves

Apart from the thermophysical properties associated with the materials, there are three control variables that define the experiment, namely, the voltage applied across the metal electrodes, ΔV , the spacing between the metal electrodes, L, and the mean concentration of the electrolyte solution, $c_{\rm ref}$. The output variables of the nonlinear model are the concentration and potential fields, as well as the surface morphology of the electrodes. More specifically, the output variable from a linear stability analysis will be the relationship between the growth constant, σ , and the wavenumber, k. These output variables are functions of the dimensionless groups, \mathcal{A} , \mathcal{B} , and \mathcal{C} .

Following the work of BuAli et al. [11], two approximations which are helpful in simplifying the forthcoming analysis will be made. Neither approximation is essential, but both taken together greatly simplify the DC problem and allow one to obtain an analytical formula for the growth rate of the instability [11]. These approximations are (i) elimination of domain dynamics in Eq. (1) and (ii) replacement of the concentration field in the term $\nabla \cdot (c\nabla \phi)$ in Eq. (1) and in the corresponding term of Eq. (2) by the mean electrolyte concentration. The first of these approximations is justified by BuAli et al. by observing that the instability is principally driven by the interfacial dynamics expressed by the Butler-Volmer equations, i.e., Eqs. (3) and (4). We continue to enforce this approximation under the assumption that the scaled frequency of forcing in the current study is low. In other words, $\Omega \equiv \omega L^2/D < 1$, where ω is the dimensional forcing frequency. The second approximation is similar to an approach taken by Chandrasekhar [25] in the hydrodynamic instability of Taylor–Couette flows in the thin gap limit. In the current study, it is simply a heuristic approximation and justified by BuAli et al. [11] on the basis that it does not significantly change either the base or the stability results of the complete electrodeposition problem. We proceed on the basis of these approximations so as to retain algebraic simplicity without sacrificing essential physics. Like BuAli et al., we show that the model with and without these two additional approximations provide results which are close to one another. Evidence to this effect is graphically represented for typical input variables in a figure in a subsequent Sect. (cf. Fig. 3). The main equations for the concentration and potential fields for the model retaining these approximations are now:



$$\nabla^2 c = 0 \quad \text{and} \quad \nabla^2 \phi = 0, \tag{5}$$

in the domain and

$$\mathbf{n} \cdot \nabla c = -2\mathbf{n} \cdot (\mathbf{U} + \mathcal{C}\mathbf{u})$$
 and $\mathbf{n} \cdot \nabla \phi = -2\mathcal{Z}\mathbf{n} \cdot (\mathbf{U} + \mathcal{C}\mathbf{u}),$ (6)

at the boundaries, along with the Butler-Volmer equations, i.e., Eqs. (3) and (4).

2.2 Linear stability analysis

We present in brief the analysis carried out by BuAli et al. as this forms the basis for the current work. A solution of the nonlinear model is the base state, wherein the planar electrodes move at a constant speed with respect to the fixed laboratory frame. Thereafter, denoting the variables associated with the base state with an overbar and the perturbed variables with a prime, we expand the variables as

$$c = \overline{c} + \epsilon c' e^{ikx}, \quad \phi = \overline{\phi} + \epsilon \phi' e^{ikx}, \quad \text{and} \quad Y^{(j)} = \overline{Y}^{(j)} + \epsilon Y'^{(j)} e^{ikx},$$
 (7)

where j: A, C and where k is the wavenumber of the perturbation of infinitesimal amplitude, ϵ .

2.2.1 Steady base solution at $\mathcal{O}\left(\epsilon^{0}\right)$

Observing that the electrode surfaces are planar in the base state, the ion concentration and potential in the electrolyte then satisfy the following equations:

$$\frac{\mathrm{d}^2 \overline{c}}{\mathrm{d} v^2} = 0 \quad \text{and} \quad \frac{\mathrm{d}^2 \overline{\phi}}{\mathrm{d} v^2} = 0 \quad \text{in the domain } 0 < y < 1, \tag{8}$$

and

$$\frac{d\overline{c}}{dy} = -2U$$
 and $\frac{d\overline{\phi}}{dy} = -2\mathcal{Z}U$ at $y = 0$ and $y = 1$. (9)

Solving the above equations, we obtain

$$\overline{c} = -2Uy + \overline{c}^A$$
 and $\overline{\phi}^C - \overline{\phi}^A = -2\mathcal{Z}U$. (10)

Here, \overline{c}^A denotes the base concentration at the anode (y=0). It can be determined in terms of U from the definition of average concentration, i.e., $\int_0^1 \overline{c} \, dy = 1$, to obtain $\overline{c}^A = 1 + U$. This then yields the base concentration at the cathode (y=1), denoted by \overline{c}^C , as $\overline{c}^C = 1 - U$.

The unknown, U, and electrical potential can be determined from the two Butler–Volmer equations, one at each electrode. Thus, at the anode (y=0), we have

$$\mathcal{B}U = e^{[1-\beta]\left[V^A - \overline{\phi}^A - \Delta_{\text{ref}}\right]} - \overline{c}^A e^{-\beta\left[V^A - \overline{\phi}^A - \Delta_{\text{ref}}\right]},\tag{11}$$

and at cathode (y = 1), we have

$$-\mathcal{B}U = e^{[1-\beta]\left[V^C - \overline{\phi}^C - \Delta_{ref}\right]} - \overline{c}^C e^{-\beta\left[V^C - \overline{\phi}^C - \Delta_{ref}\right]}.$$
(12)



16 Page 8 of 18 A. Ganesh et al.

Combining Eq. (10) and the Butler-Volmer equations, an implicit equation for U is obtained as

$$-\mathcal{B}U[f(U)]^{\beta} - f(U) + 1 - U = 0 \tag{13}$$

where $f(U) = \frac{(1-U)+(1+U)\mathrm{e}^{-\beta(V-2\mathcal{Z}U)}}{1+\mathrm{e}^{(1-\beta)(V-2\mathcal{Z}U)}}$, where V is used as a short form for ΔV .

2.2.2 Perturbed state solution at $\mathcal{O}(\epsilon)$

The domain equations at the first-order perturbation are

$$\frac{\partial^2 c'}{\partial y^2} - k^2 c' = 0 \quad \text{and} \quad \frac{\partial^2 \phi'}{\partial y^2} - k^2 \phi' = 0, \tag{14}$$

and at the two-electrode surfaces, we have

$$\frac{\partial c'}{\partial y} = -2\mathcal{C}\frac{\mathrm{d}Y'}{\mathrm{d}t} \quad \text{and} \quad \frac{\partial \phi'}{\partial y} = -2\mathcal{Z}\mathcal{C}\frac{\mathrm{d}Y'}{\mathrm{d}t}. \tag{15}$$

Defining \overline{c}^{*A} and \overline{c}^{*C} as

$$\bar{c}^{*A} = [1 - \beta] e^{[V^A - \bar{\phi}^A - \Delta_{\text{ref}}]} + \beta \bar{c}^A, \tag{16a}$$

and

$$\overline{c}^{*C} = [1 - \beta] e^{[V^C - \overline{\phi}^C - \Delta_{\text{ref}}]} + \beta \overline{c}^C, \tag{16b}$$

we obtain the Butler-Volmer equations at the anode and cathode as

$$\left[\frac{\overline{c}^{*A} - \overline{c}^{A}}{(1 - \beta)U}\right] \mathcal{C}\frac{\mathrm{d}Y'^{A}}{\mathrm{d}t} + \left[\overline{c}^{*A}\phi'^{A} + c'^{A}\right] = -Y'^{A}\left[-2\mathcal{Z}U\overline{c}^{*A} - 2U\right] + \overline{c}^{*A}\mathcal{A}k^{2}Y'^{A},\tag{17a}$$

and

$$\left[\frac{\overline{c}^{*C} - \overline{c}^C}{(1 - \beta)U}\right] \mathcal{C}\frac{\mathrm{d}Y'^C}{\mathrm{d}t} + \left[\overline{c}^{*C}\phi'^C + c'^C\right] = -Y'^C\left[-2\mathcal{Z}U\overline{c}^{*C} - 2U\right] - \overline{c}^{*C}\mathcal{A}k^2Y'^C. \tag{17b}$$

Solving for c' and ϕ' from Eqs. (14) and (15) and evaluating them at the anode and the cathode, we get

$$c'^{A} = \frac{2\mathcal{C}}{k \sinh k} \left[\frac{\mathrm{d}Y'^{A}}{\mathrm{d}t} \cosh k - \frac{\mathrm{d}Y'^{C}}{\mathrm{d}t} \right],\tag{18a}$$

$$c^{\prime C} = \frac{2\mathcal{C}}{k \sinh k} \left[\frac{\mathrm{d}Y^{\prime A}}{\mathrm{d}t} - \frac{\mathrm{d}Y^{\prime C}}{\mathrm{d}t} \cosh k \right],\tag{18b}$$

$$\phi'^{A} = \frac{2\mathcal{Z}\mathcal{C}}{k \sinh k} \left[\frac{\mathrm{d}Y'^{A}}{\mathrm{d}t} \cosh k - \frac{\mathrm{d}Y'^{C}}{\mathrm{d}t} \right],\tag{19a}$$



and

$$\phi'^{C} = \frac{2\mathcal{Z}\mathcal{C}}{k \sinh k} \left[\frac{\mathrm{d}Y'^{A}}{\mathrm{d}t} - \frac{\mathrm{d}Y'^{C}}{\mathrm{d}t} \cosh k \right],\tag{19b}$$

whence, further substitution into Eqs. (17a) and (17b), we get

$$\left[\frac{\overline{c}^{*A} - \overline{c}^{A}}{(1 - \beta)U}\right] \mathcal{C}\frac{dY'^{A}}{dt} + \frac{2\mathcal{C}}{k \sinh k} \left[\frac{dY'^{A}}{dt} \cosh k - \frac{dY'^{C}}{dt}\right] \left[1 + 2\overline{c}^{*A}\right] + Y'^{A} \left[-2U - 2\mathcal{Z}U\overline{c}^{*A} - \overline{c}^{*A}\mathcal{A}k^{2}\right] = 0,$$
(20a)

and

$$\left[\frac{\overline{c}^{*C} - \overline{c}^{C}}{(1 - \beta)U}\right] \mathcal{C}\frac{dY'^{C}}{dt} + \frac{2\mathcal{C}}{k \sinh k} \left[\frac{dY'^{A}}{dt} - \frac{dY'^{C}}{dt} \cosh k\right] \left[1 + 2\overline{c}^{*C}\right] + Y'^{C} \left[-2U - 2\mathcal{Z}U\overline{c}^{*C} + \overline{c}^{*C}\mathcal{A}k^{2}\right] = 0.$$
(20b)

Equations (20a) and (20b) are at the heart of the problem. They are, in principal, two equations for the perturbed electrode deviations, Y'^A and Y'^C . In the typical instability problem, where we only have DC forcing, the perturbed variables, c', ϕ' , and Y' are re-expanded as $c'e^{\sigma t}$, $\phi'e^{\sigma t}$, etc., where σ is termed the growth constant and the primed notation is retained for simplicity. Introducing these re-expanded variables into the above and, in particular, into Eqs. (20a) and (20b) yield two algebraic equations that constitute an eigenvalue problem with $\{Y'^A, Y'^C\}$ as the eigenvector and σ as the eigenvalue. These equations, obtained at $\mathcal{O}(\epsilon)$, are in the form $A\Psi = \sigma B\Psi$, where A and B are 2×2 matrices. This yields a quadratic equation for σ , the eigenvalue, with one of the roots being negative and the other root being positive for some values of k^2 and negative beyond a critical value of k^2 . The eigenvector, $\Psi = \{Y'^A, Y'^C\}$ will reveal that Y'^A/Y'^C is typically very small, indicating insignificant morphological growth at the anode compared to the cathode, in agreement with the physical argument proposed in the introduction. In Fig. 3, typical plots of U vs Vfrom Eq. (13) and σ vs k^2 from the solutions of (20a) and (20b), based on our principal approximations, are given. The figure also depicts the corresponding curves from the full model without these approximations, repeating the work given by BuAli et al. As is clear, the simplified model provides a reasonable approximation to the full model. Observe in particular, that the wavelength corresponding to the maximum growth rate remains virtually unchanged, while the neutral point has shifted to lower wavenumber indicating that the approximation leads to a slightly lower range of unstable wavenumbers. The closeness between these two models encourages us to continue on the basis of Eqs. (3), (4), (5), and (6). To this end, we consider the superposition of a small voltage input on a base DC voltage.

3 Small-amplitude AC voltage superimposed on a base DC voltage

Let us now assume that an additional AC voltage of very small amplitude, δ , is imposed on the base DC voltage, i.e., $V^A = V_0^A + \delta V_1^A$ and $V^C = V_0^C + \delta V_1^C$, where $V_1^A = \cos \Omega t$ and $V_1^C = 0$. We will see later that the case of equivalent root mean square (RMS) DC voltage, obtained by setting $V_1^A = 1/\sqrt{2}$ and $V_1^C = 0$, is of special significance, when comparing the effect of AC input with the companion DC problem.

In order to determine the effect of the additional small amplitude voltage on the base DC problem, we expand the base state variables (denoted generically by $\overline{\zeta}$), the perturbed state variables (denoted by ζ'), as well as the growth constant, σ , in series of δ as follows:



16 Page 10 of 18
A. Ganesh et al.

$$\overline{\zeta} = \overline{\zeta}_0 + \delta \, \overline{\zeta}_1 + \frac{\delta^2}{2} \, \overline{\zeta}_2 + \cdots, \quad \zeta' = \zeta'_0 + \delta \zeta'_1 + \frac{\delta^2}{2} \zeta'_2 + \cdots \quad \text{and} \quad \sigma = \sigma_0 + \delta \, \sigma_1 + \frac{\delta^2}{2} \, \sigma_2 + \cdots$$
 (21)

As the additional voltage is of a time-periodic AC form, further expansions using Floquet theory [23,24] are done for the base state and perturbed state variables, as below:

$$\overline{\zeta} = \overline{\zeta}_0 + \delta \sum_{n=-N}^{N} \overline{\zeta}_{1n} e^{in\Omega t} + \frac{\delta^2}{2} \sum_{n=-N}^{N} \overline{\zeta}_{2n} e^{in\Omega t},$$
(22a)

$$\zeta' = \zeta_0' + \delta \sum_{n = -N}^{N} \zeta_{1n}' e^{in\Omega t} + \frac{\delta^2}{2} \sum_{n = -N}^{N} \zeta_{2n}' e^{in\Omega t}, \tag{22b}$$

where N determines the cut-off frequency in the Fourier series expansion. These expansions are then substituted into the base state equations, at $\mathcal{O}(\epsilon)$, and perturbed state equations, at $\mathcal{O}(\epsilon)$. Collecting terms at each order of δ , we obtain corrections to the base state solution, as well as the perturbed state solution. We, thus, get at $\mathcal{O}(\delta^0)$:

$$\underline{A_0} \ \underline{\Psi_0'} - \sigma_0 \ \underline{B_0} \ \underline{\Psi_0'} = 0, \tag{23a}$$

at $\mathcal{O}(\delta)$:

$$\underline{A_0} \, \underline{\Psi_1'} - \sigma_0 \, \underline{B_0} \, \underline{\Psi_1'} = \sigma_0 \, \underline{B_1} \, \underline{\Psi_0'} + \sigma_1 \, \underline{B_0} \, \underline{\Psi_0'} - \underline{A_1} \, \underline{\Psi_0'}, \tag{23b}$$

and at $\mathcal{O}(\delta^2/2)$:

$$\underline{\underline{\underline{A_0}}} \underline{\underline{\Psi_2'}} - \sigma_0 \underline{\underline{\underline{B_0}}} \underline{\underline{\Psi_2'}} = \sigma_0 \underline{\underline{\underline{B_2}}} \underline{\underline{\Psi_0'}} + 2\sigma_0 \underline{\underline{\underline{B_1}}} \underline{\underline{\Psi_1'}} + 2\sigma_1 \underline{\underline{\underline{B_1}}} \underline{\underline{\Psi_0'}} + 2\sigma_1 \underline{\underline{\underline{B_0}}} \underline{\underline{\Psi_1'}} + 2\sigma_1 \underline{\underline{\underline{B_0}}} \underline{\underline{\Psi_1'}} + 2\sigma_1 \underline{\underline{\underline{B_0}}} \underline{\underline{\Psi_1'}} + 2\sigma_1 \underline{\underline{\underline{B_0}}} \underline{\underline{\Psi_1'}}$$

$$+ \sigma_2 \underline{\underline{\underline{B_0}}} \underline{\underline{\Psi_0'}} - 2\underline{\underline{\underline{A_1}}} \underline{\underline{\Psi_1'}} - \underline{\underline{A_2}} \underline{\underline{\Psi_0'}}.$$

$$(23c)$$

In the above, the unknowns are σ_0 and $\underline{\Psi_0'}$ at $\mathcal{O}\left(\delta^0\right)$, σ_1 and $\underline{\Psi_1'}$ at $\mathcal{O}(\delta)$ and σ_2 and $\underline{\Psi_2'}$ at $\mathcal{O}(\delta^2/2)$. The vectors, Ψ_0' , Ψ_1' and Ψ_2' take different forms. They are given by

$$\underline{\Psi}_{0}^{'} = \begin{bmatrix} Y_{01}^{'A} \\ Y_{02}^{'A} \\ \vdots \\ Y_{0n}^{'A} \\ Y_{01}^{'C} \\ Y_{02}^{'C} \\ \vdots \\ Y_{0n}^{'C} \end{bmatrix}, \quad \underline{\Psi}_{1}^{'} = \begin{bmatrix} Y_{11}^{'A} \\ Y_{12}^{'A} \\ \vdots \\ Y_{1n}^{'C} \\ Y_{12}^{'C} \\ \vdots \\ Y_{1n}^{'C} \end{bmatrix}, \quad \text{and} \quad \underline{\Psi}_{2}^{'} = \begin{bmatrix} Y_{21}^{'A} \\ Y_{22}^{'A} \\ \vdots \\ Y_{2n}^{'A} \\ Y_{2n}^{'C} \\ Y_{22}^{'C} \\ \vdots \\ Y_{2n}^{'C} \end{bmatrix}. \tag{24}$$

The matrices, $\underline{\underline{A_i}}$, $\underline{\underline{B_i}}$ above contain involved algebraic expressions and are given in the supplementary material to this manuscript. The perturbations to the growth constant at various order, σ_1 and σ_2 , are the key unknowns that we seek from the above equations. They are obtained by solvability conditions by observing that the right hand sides of Eqs. (23b) and (23c) must reside in the null space of the adjoint of Eq. (23a). The solvability conditions require numerical projection of the right hand side vectors on to the null space. These were done using *Mathematica* v.12.0 and for a representative electrodeposition system whose properties are given in Table 1 and in dimensionless form in Table 2. We now turn to a discussion of results from these calculations.



4 Results

An important observation is that σ_1 becomes zero. This comes as no surprise as the mean of an AC input is zero and periodic inputs are symmetric about the mean. Another important observation is that our results at every order has been computationally seen to be independent of Ω . We attribute this observation to the assumption that $\Omega < 1$. This in turn implies that the domain dynamics are slaved to the interface dynamics and are in phase with the periodicity of the interface motion. A third observation is that the second order correction the base speed, U_2 vs. V_0 is key to the behavior of the second order correction to growth rate, σ_2 . This is explained as follows. At each order of the calculation, of interest are the time-averaged perturbations to the base speed, i.e., U_1 and U_2 . The time-averaged U_1 is zero for the AC perturbation. Figure 4a depicts the base U_0 vs V_0 and Fig. 4b depicts the corresponding second order correction U_2 vs V_0 , for three different values of \mathcal{B} . These values are chosen for typical electrode spacings given in Table 2. When the U_0-V_0 curve is of negative curvature (cf. dashed curve in Fig. 4a), U_2 is strictly negative (cf. dashed curves in Fig. 4b), whereas, when the U_0-V_0 curve has an inflection point indicating a change in curvature (cf. solid curve in Fig. 4a), U_2 correspondingly changes sign (cf. solid curves in Fig. 4b). The critical value of \mathcal{B} , which just marks the appearance of an inflection point on the U_0-V_0 curve is given by $\mathcal{B}_c = 3.3723$ (dotted curve). This critical value, \mathcal{B}_c , can be obtained from Eq. ((13)) by setting the slope of the curvature of U_0-V_0 curve at origin (U=V=0) to zero, i.e., $\frac{\partial^3 U_0}{\partial V_0^3}(V_0=0)=0$. Differentiating Eq. (13) once with respect to V, we obtain

$$\frac{\partial U_0}{\partial V_0}(V_0 = 0) = \frac{1}{(2\mathcal{B} + 4)}. (25)$$

In obtaining Eq. (25), we have used $\beta = 1/2$ and Z = 1, as given in Table 1. Differentiating Eq. (13) twice and making use of (25), we obtain

$$\frac{\partial^2 U_0}{\partial V_0^2}(V_0 = 0) = 0,\tag{26}$$

independent of \mathcal{B} . This is also evident from Fig. 4b, where for all choices of \mathcal{B} , it is seen that $U_2(V=0)=0$. Finally, differentiating (13) thrice, substituting (25) and (26), and setting $\frac{\partial^3 U_0}{\partial V_0^3}(V_0=0)=0$, we obtain the following cubic equation for \mathcal{B}_c ,

$$\mathcal{B}_c^3 - 9\mathcal{B}_c - 8 = 0. (27)$$

Solving the above equation for the only positive physically meaningful root, we get $B_c = 3.3723$.

The change in curvature in U_0-V_0 curve as a function of \mathcal{B} demands an explanation. Low values of \mathcal{B} typically occur at large electrode spacing and indicate diffusion-limited transport. Ions released at the anode, on account of the applied voltage, diffuse through the solution without charge accumulation at the cathode for all values of voltage input until the voltage becomes large enough that a limiting current is achieved. Contrast this with the case of small electrode spacing, i.e., large \mathcal{B} . Here, diffusional transport is not limiting and small voltage input results in charge accumulation until the voltage input is made strong enough that diffusional transport and kinetic conversion become comparable. Further increase in the applied voltage leads to the total current and electrode speed approaching their limiting values. This dual effect of applied voltage on diffusional transport and reaction kinetics, which is seen at large \mathcal{B} , is the principal cause for the presence of an inflection point. It might be noted that the topology of the U_0-V_0 curves as a function of the parameter \mathcal{B} is independent of the approximations made in the model from which Eq. (13) arises (cf. Fig. 3a).

Note that at every point on the base curve, Fig. 4a, σ_0 vs k^2 and likewise σ_2 vs k^2 may be plotted. In particular, four markers are placed on the solid curve, the curve of changing curvature. These four markers have been chosen to exemplify four different characteristics of the σ_2 vs k^2 curves displayed in Fig. 5. Observe that in the first pair, i.e.,



16 Page 12 of 18 A. Ganesh et al.

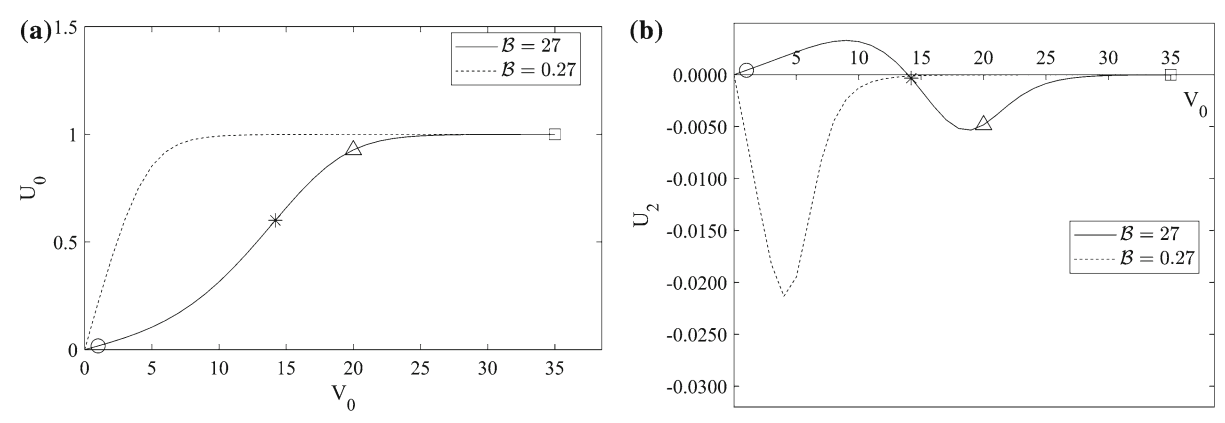


Fig. 4 a U_0 as a function of the base voltage, V_0 . b Time-averaged component of U_2 as a function of the base voltage, V_0 ; solid curve: $\mathcal{B}=27$, dotted: $\mathcal{B}_c=3.3723$, dashed curve: $\mathcal{B}=0.27$. U_2 is always negative for the dashed curve, while changes sign at $V_0\sim14$ for the solid curve. The critical value of $\mathcal{B}_c=3.3723$ marks the transition with zero slope for U_2 at $V_0=0$. The markers on the $\mathcal{B}=27$ curve correspond to the particular cases of interest discussed in Fig. 5

Fig. 5a and b, drawn for the lowest marker of Fig. 4a, denoted by a circle (\circ), the σ_2 vs k^2 curve follows the same behavior as the σ_0 vs k^2 curve. Contrast that with the second marker, denoted by a star (*), located slightly above the inflection point. Here, the σ_2 vs k^2 curve given by Fig. 5d is a positive correction on the σ_0 vs k^2 curve shown in Fig. 5c. In both cases considered above, it should be noted that the erstwhile unstable wavenumbers are further destabilized. The last two markers denoted by (Δ) and (\Box) in Fig. 4a have their σ_2 vs k^2 curves displayed in Fig. 5f and h respectively. They both show an initial negative correction which then changes sign. The value of the voltage, where the σ_2 vs k^2 curve moves from the positive half plane to the negative half plane is not precisely where U_2 changes sign in Fig. 4b. The location where U_2 changes sign precedes the location where the σ_2 vs k^2 curve moves from being wholly positive to negative. This is important because a negative value of σ_2 implies stabilization of an otherwise unstable morphology of the electrodes. It is clear from these exemplifying calculations that the AC perturbation can either have a stabilizing or destabilizing effect, depending upon the base DC voltage and the value of \mathcal{B} . An observation made from Fig. 5e and f is that the long-wave perturbations can be selectively stabilized by AC forcing, thereby possibly leading either to well-defined patterns or regularized dendritic patterns. Such regularization of dendritic side-branching by periodic forcing has been observed experimentally and numerically in the case of solidification [26]. Further, a comparison of Fig. 5g and h show the stabilizing effect of AC perturbation for all erstwhile unstable wavenumbers, suggesting the hypothesis that large amplitude AC forcing can completely quench the instability. A formal proof for this hypothesis, however, is beyond the scope of the current work. It must be noted that the correction to the growth constant is sizeable for the system exemplified in this study in panels 5g and 5h. However, calculations reveal that the correction may be amplified for systems with low magnitudes of C. In the case of small amplitude AC perturbations, we aim to understand the root cause of the behavior of σ_2 vs k^2 , the leading order correction to the growth constant, and it is to this that we proceed next.

Physical insights into the AC problem from the companion DC problem

Ordinarily, the effect of a DC perturbation on a base DC voltage can be obtained by merely recalculating the DC problem with an increased input. However, to see the effect of this increased DC applied voltage, we make the same algebraic moves as we did in the AC case, and compare our results with the corresponding AC problem. The calculations from such an analysis are revealed in Fig. 6. Figure 6a is a comparison of the time-averaged value of U_2 in the AC case with the corresponding value of U_2 in the RMS DC case. This is indicative that the predictions of the one case can be made entirely from the other for all even orders of δ . Figure 6b reveals the same result, but in this case for σ_2 vs k^2 . This relationship between the AC forcing and the DC forcing carries through for all values of applied voltage and all topologies of σ_2 vs k^2 given in Fig. 5. Also from Fig. 5, it is evident that the shift in σ_2 vs k^2 curves from positive half plane to negative half plane exhibits its signature at small k. Thus, an investigation of the limit of small k is expected to shed light into the aforementioned transition in σ_2 vs k^2 curves. Because the DC



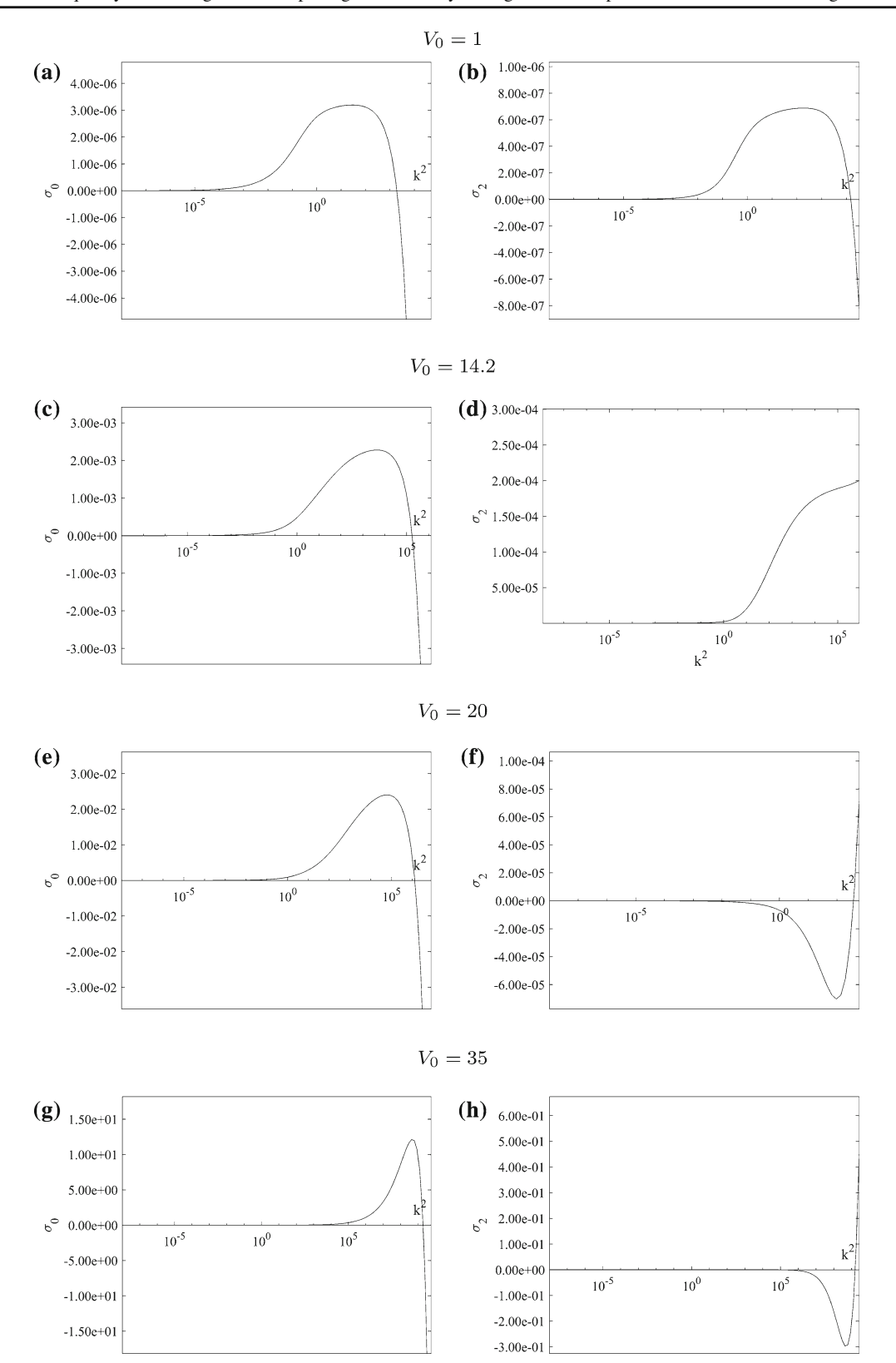


Fig. 5 The effect of small AC voltage on the linear growth rate plotted for different values of imposed base DC voltage. Panels (**a**, **c**, **e**, **g**) depict the corresponding σ_0 as function of k^2 and panels (**b**, **d**, **f**, **h**) depict σ_2 as function of k^2 ; $\mathcal{B} = 27$

6 Page 14 of 18 A. Ganesh et al.

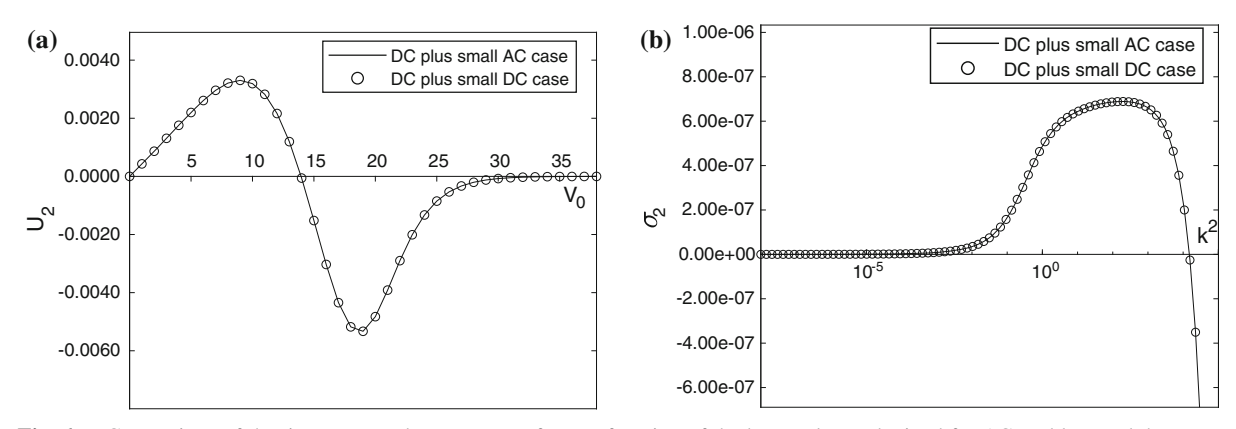


Fig. 6 a Comparison of the time-averaged component of U_2 as function of the base voltage obtained for AC problem and the corresponding RMS DC case; $\mathcal{B} = 27$. b Comparison of the σ_2 vs k^2 curve obtained for AC problem and the corresponding RMS DC case; $V_0 = 1$, $\mathcal{B} = 27$

problem is a forerunner at every even order of the AC problem, it is instructive to investigate the limiting case of small k in the DC problem in order to gain insight into the corresponding AC problem. An additional assumption of small U is required to render the problem amenable to analytical treatment.

4.1 The limiting case of small k and U

An analytical expression for σ in terms of the base variable U may be used to obtain an estimate of the sign of σ_2 in the limit of small k. We further assume that the base electrode speed, U, is also small.

Notice that for a pure DC problem σ can be calculated from the quadratic expression,

$$(1+M)\sigma^2 - (\sigma_A + \sigma_C)\sigma + \sigma_A\sigma_C = 0, (28)$$

where

$$M = \frac{\frac{4\left[1+2\overline{c}^{*C}\right]\left[1+2\overline{c}^{*A}\right]}{k^{2}\sinh^{2}k}}{\left(\frac{\overline{c}^{*A}-\overline{c}^{A}}{(1-\beta)U} + \frac{2\cosh k\left[1+2\overline{c}^{*A}\right]}{k\sinh k}\right)\left(\frac{\overline{c}^{*C}-\overline{c}^{C}}{(1-\beta)U} - \frac{2\cosh k\left[1+2\overline{c}^{*C}\right]}{k\sinh k}\right)},$$

$$\mathcal{C}\sigma_{A} = \frac{-\left[-2U - 2\mathcal{Z}U\overline{c}^{*A} - \mathcal{A}k^{2}\overline{c}^{*A}\right]}{\left(\frac{\overline{c}^{*A}-\overline{c}^{A}}{(1-\beta)U} + \frac{2\cosh k\left[1+2\overline{c}^{*A}\right]}{k\sinh k}\right)},$$

and

$$\mathfrak{C}\sigma_C = \frac{-\left[-2U - 2\mathcal{Z}U\overline{c}^{*C} + \mathcal{A}k^2\overline{c}^{*C}\right]}{\left(\frac{\overline{c}^{*C} - \overline{c}^C}{(1-\beta)U} - \frac{2\cosh k\left[1 + \mathcal{Z}\overline{c}^{*C}\right]}{k\sinh k}\right)}.$$

To see how we arrive at Eq. (28), substitute $Y^{'C} = 0$ in Eq. (20a), solve for σ and name it σ_A . Likewise, solve Eq. (20b) for σ upon inserting $Y^{'A} = 0$, and call this root σ_C . Equations (20a) and (20b) are a quadratic equation for σ , which upon algebraic manipulation can be conveniently represented in terms of σ_A and σ_C . This results in Eq. (28), where it might be observed that the variables, σ_A , σ_C and M are known explicitly in terms of k and k, which, in turn, derives from Eq. (13). The two roots of σ from Eq. (28) are precisely the dashed curves displayed in Fig. 3b.



Recall that \overline{c}^A and \overline{c}^C are 1+U and 1-U respectively and \overline{c}^{*A} and \overline{c}^{*C} are given by Eqs. (16a) and (16b). They can be expanded for small U holding \mathcal{B} fixed. These expansions allow us to obtain limiting forms for M, σ_A and σ_C , whence we arrive at simple expressions for the roots of Eq. (28). Thereafter, the base speed, U, is expanded about $\delta=0$ with the objective of finding the first and second order corrections to σ , i.e., σ_1 and σ_2 . We now proceed to give the main results.

4.1.1 Expansions in terms of small U

In the limit of small U, the variables, σ_A , σ_C and (1 + M), take the limiting forms:

$$\sigma_A = \frac{Uk^2}{\mathcal{C}} \left[1 - k^2 \left(\frac{1}{3} + F_1 \right) \right],\tag{29a}$$

$$\sigma_C = -\frac{Uk^2}{\mathcal{C}} \left[1 - k^2 \left(\frac{1}{3} - F_2 \right) \right],\tag{29b}$$

$$(1+M) = k^2 \left[1 + F_1 - F_2 - k^2 \left\{ \frac{2}{3} + \frac{4}{3} (F_1 - F_2) + F_1 F_2 + (F_1 - F_2)^2 \right\} \right], \tag{29c}$$

where

$$F_{1} = \frac{\frac{\overline{c}^{*A} - \overline{c}^{A}}{(1 - \beta)U}}{2\left[1 + Z\overline{c}^{*A}\right]} = \frac{\mathcal{B}}{4}\left[1 + U\frac{\mathcal{B}}{4} - U^{2}\left(\frac{1}{2} + \frac{\mathcal{B}}{4} + \frac{\mathcal{B}^{2}}{16}\right) + U^{3}\left(\frac{1}{16} + \frac{3\mathcal{B}}{16} + \frac{\mathcal{B}^{2}}{16} - \frac{3\mathcal{B}^{3}}{64}\right)\right],$$

and

$$F_2 = \frac{\frac{\overline{c}^{*C} - \overline{c}^C}{(1 - \beta)U}}{2\left[1 + Z\overline{c}^{*C}\right]} = \frac{\mathcal{B}}{4}\left[-1 + U\frac{\mathcal{B}}{4} + U^2\left(\frac{1}{2} + \frac{\mathcal{B}}{4} + \frac{\mathcal{B}^2}{16}\right) + U^3\left(\frac{1}{16} + \frac{3\mathcal{B}}{16} + \frac{\mathcal{B}^2}{16} - \frac{3\mathcal{B}^3}{64}\right)\right].$$

It is observed that $\sigma_A + \sigma_C \approx 0$, whence $\sigma^2 = -\frac{\sigma_A \sigma_C}{1+M}$ is a consequence of Eq. (28). Taking only the leading order term for the dominant σ up to $\mathcal{O}(U^3)$, we obtain

$$\sigma = -\frac{Uk}{\mathcal{C}\left(1 + \frac{\mathcal{B}}{2}\right)^{1/2}} \left[1 + \frac{U^2}{2 + \mathcal{B}} \left(\frac{\mathcal{B}}{16} + \frac{\mathcal{B}^2}{8} + \frac{\mathcal{B}^3}{32} \right) \right]. \tag{30}$$

Equation (30) is not only an expression up to $\mathcal{O}\left(U^3\right)$, it also corrects the low k limit expression obtained by BuAli et al. [11]. Note in the above that \mathcal{C} is a negative parameter, so the dominant σ must be positive. The base speed, U, may be expanded in terms of δ leading to corrections to the dominant σ , given by Eq. (30). We therefore have $U = U_0 + \delta U_1 + \frac{\delta^2}{2} U_2$, whence at $\mathcal{O}\left(\delta^0\right)$, we get

$$\sigma_0 = -\frac{U_0 k}{\mathcal{C} \left(1 + \frac{\mathcal{B}}{2} \right)^{1/2}} \left[1 + \frac{U_0^2}{2 + \mathcal{B}} \left(\frac{\mathcal{B}}{16} + \frac{\mathcal{B}^2}{8} + \frac{\mathcal{B}^3}{32} \right) \right]. \tag{31a}$$

At $\mathcal{O}(\delta)$, we get

$$\sigma_1 = -\frac{U_1 k \left[64 + 32\mathcal{B} + 6\mathcal{B} U_0^2 + 12\mathcal{B}^2 U_0^2 + 3\mathcal{B}^3 U_0^2 \right]}{16\mathcal{C}\sqrt{2}(2+\mathcal{B})^{3/2}},\tag{31b}$$



16 Page 16 of 18 A. Ganesh et al.

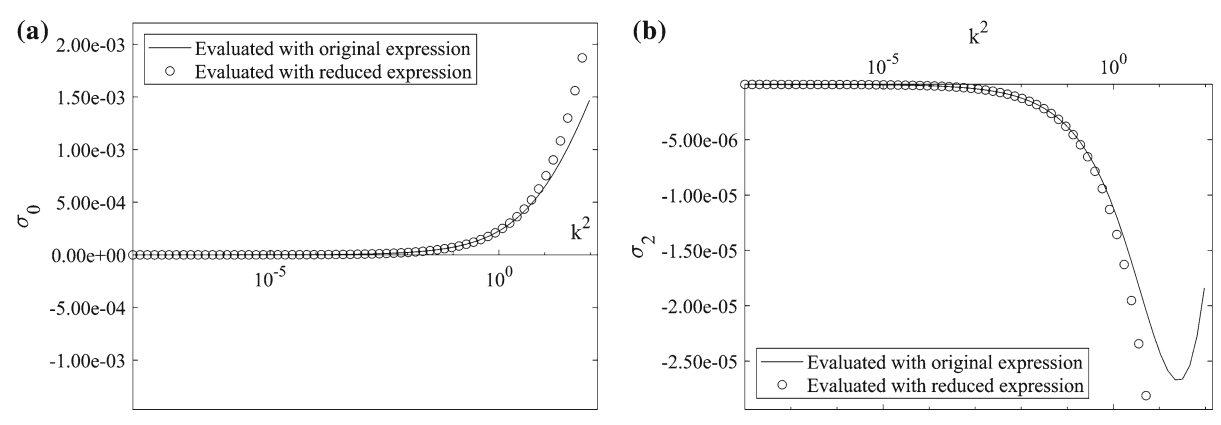


Fig. 7 Comparison of the linear growth rate predicted by our simplified analytical expression in the limit of low U and k with the full solution. The markers denote the reduced expression while the curve denotes the full solution. $\mathbf{a} \ \sigma_0$ as function of k^2 , $\mathbf{b} \ \sigma_2$ as function of k^2 ; $V_0 = 1$, $\mathcal{B} = 0.27$, resulting in $U_0 = 0.218$

and at $\mathcal{O}(\delta^2/2)$, we get

$$\sigma_{2} = \underbrace{-\frac{k \left[12\mathcal{B}U_{0}U_{1}^{2} + 24\mathcal{B}^{2}U_{0}U_{1}^{2} + 6\mathcal{B}^{3}U_{0}U_{1}^{2} + 64U_{2} + 32\mathcal{B}U_{2} + 6\mathcal{B}U_{0}^{2}U_{2} + 12\mathcal{B}^{2}U_{0}^{2}U_{2}\right]}_{\text{Term I}}$$

$$\underbrace{-\frac{k \left[3\mathcal{B}^{3}U_{0}^{2}U_{2}\right]}{16\mathcal{C}\sqrt{2}(2+\mathcal{B})^{3/2}}}_{\text{Term I}}.$$
(31c)

The sign of σ_2 depends on the magnitude of \mathcal{B} . In the limit of small \mathcal{B} , Eq. (30) reduces to

$$\sigma = -\frac{Uk}{\varrho}.\tag{32}$$

Correspondingly, Eq. (31c) reduces to

$$\sigma_2 = -\frac{U_2 k}{c}.\tag{33}$$

In this case, U_2 is negative (cf. the dashed curve in Fig. 4b), thus σ_2 is also negative as evident from Eq. (33) and depicted in Fig. 7b. Now, for the case of large \mathcal{B} , σ_2 has to be determined using Eq. (31c). For this case, we know that U_2 is positive in the low U limit, as seen from solid curve in Fig. 4b. Thus, the entirety of Terms I and II are strictly positive, which makes σ_2 positive (cf. Fig. 8b). The change in sign in σ_2 in the low U limit as \mathcal{B} increases in magnitude is the essence of the results portrayed in Fig. 4b and in the inferences made therefrom.

5 Summary

This study shows that the effect of AC perturbation on the morphological instability of electrodes during electrodeposition driven by a base DC field, V, hinges on the behavior of a pure DC problem itself. This is because the timeaveraged response of a small AC perturbation of amplitude, δ , on a base DC problem is first seen at $\mathcal{O}(\delta^2)$ and arises from the RMS component. Our study specifically shows that the behavior of the base speed, U, with respect to the applied voltage, V, forecasts the conclusions that we arrive at. The nature of this behavior is principally of two types.



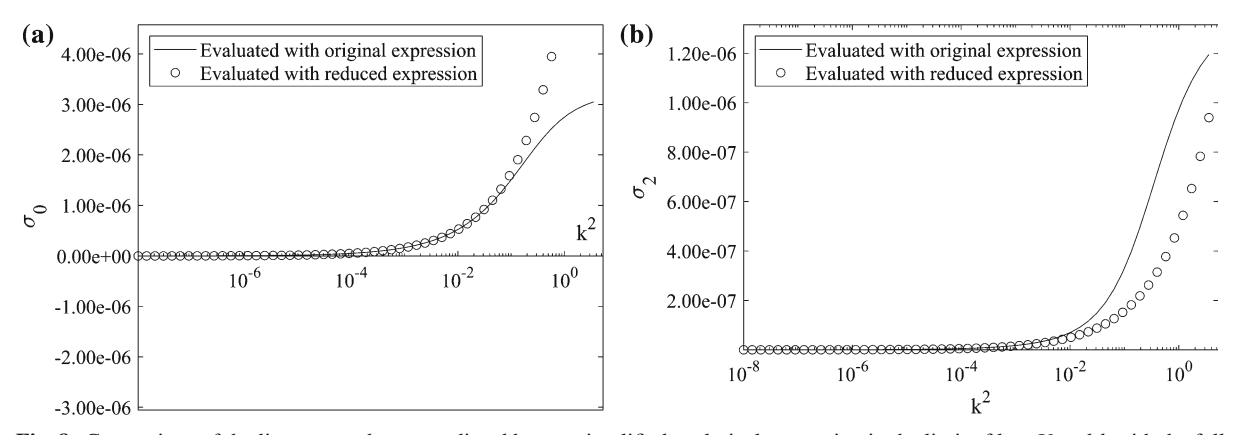


Fig. 8 Comparison of the linear growth rate predicted by our simplified analytical expression in the limit of low U and k with the full solution. The markers denote the reduced expression while the curve denotes the full solution. **a** σ_0 as function of k^2 , **b** σ_2 as function of k^2 ; $V_0 = 1$, $\mathcal{B} = 27$ resulting in $U_0 = 0.017$

When \mathcal{B} is small, indicating diffusion-limited transport or large electrode spacing, the curvature of the U-V graph is entirely negative, whereas for large \mathcal{B} , it is initially positive, advances through an inflection point, and becomes negative. The critical value of \mathcal{B} that marks the transition is analytically obtained as $\mathcal{B}_c = 3.3723$. The changing curvature for large \mathcal{B} signals a change in the relative stabilization as the voltage, V, increases. For small applied voltages, the leading order correction to the growth constant, σ , is positive and becomes negative for large applied voltages following the trend of curvature displayed in the U-V graph. These results are portrayed in this study via calculations and asymptotic expressions obtained in the limit of small wavenumber and small electrode base speed.

Acknowledgements We acknowledge financial support from NASA (NNX17AL27G), NSF (2004527), and William P. and Tracy Cirioli professorship. D.S.P. is also grateful for funding from the Initiation Grant, IIT Kanpur.

Declarations

Conflict of interest The authors declare that they have no conflict of interest.

References

- 1. Bockris J, Reddy A (1970) Modern electrochemistry, vol 2. Plenum Press, New York
- 2. Johns LE, Narayanan R (2002) Interfacial instability. Springer, New York
- Haataja M, Srolovitz DJ, Bocarsly AB (2003) Morphological stability during electrodeposition: I. Steady states and stability analysis. J Electrochem Soc 150:C699
- 4. Nielsen CP, Bruus H (2015) Morphological instability during steady electrodeposition at overlimiting currents. Phys Rev E 92:052310
- 5. Enrique RA, DeWitt S, Thornton K (2017) Morphological stability during electrodeposition. MRS Commun 7:658
- Barkey DP, Muller RH, Tobias CW (1989) Roughness development in metal electrodeposition: I. Experimental results. J Electrochem Soc 136:2199
- Barkey DP, Muller RH, Tobias CW (1989) Roughness development in metal electrodeposition: II. Stability theory. J Electrochem Soc 136:2207
- 8. Sundström LG, Bark FH (1995) On morphological instability during electrodeposition with a stagnant binary electrolyte. Electrochim Acta 5:599
- 9. de Bruyn JR (1996) Early stages of ramified growth in quasi-two-dimensional electrochemical deposition. Phys Rev E 53:R5561
- 10. Léger C, Servant L, Argoul JLBF (1999) Growth patterns in electrodeposition. Physica A 263:305
- 11. BuAli Q, Johns LE, Narayanan R (2006) The growth of roughness during electrodeposition. Electrochim Acta 51:2881
- 12. Palmer HJ (1976) The hydrodynamic stability of rapidly evaporating liquids at reduced pressure. J Fluid Mech 75:487–511
- 13. Davis SH (2001) Theory of solidification. Cambridge Monographs on Mechanics (Cambridge University Press), Cambridge



16 Page 18 of 18 A. Ganesh et al.

 Li S, Lowengrub JS, Fontana J, Palffy-Muhora P (2009) Control of viscous fingering patterns in a radial Hele–Shaw cell. Phys Rev Lett 102:174501

- McFadden GB, Coriell SR, Gurski KF, Cotrell DL (2007) Onset of convection in two liquid layers with phase change. Phys Fluids 19:104109
- 16. McFadden GB, Coriell SR (2009) Onset of oscillatory convection in two liquid layers with phase change. Phys Fluids 21:034101
- Kahanda GLMKS, Zou XQ, Farrell R, Wong PZ (1992) Columnar growth and kinetic roughening in electrochemical deposition. Phys Rev Lett 68:3741–3744
- 18. Aogaki R, Makino T (1981) Theory of powdered metal formation in electrochemistry—morphological instability in galvanostatic crystal growth under diffusion control. Electrochim Acta 26:1509
- 19. Pritzker MD, Fahidy TZ (1992) Morphological stability of a planar metal electrode during potentiostatic electrodeposition and electrodissolution. Electrochim Acta 37:49–68
- 20. Kaptiza PL (1951) Dynamic stability of a pendulum with a vibrating suspension. Soviet Phys. JETP 21:588
- Shukla PK, Narayanan R (2002) The effect of time-dependent gravity with multiple frequencies on the thermal convective stability of a fluid layer. Int J Heat Mass Transf 45:4011
- Sterman-Cohen E, Bestehorn M, Oron A (2017) Rayleigh–Taylor instability in thin liquid films subjected to harmonic vibration. Phys Fluids 29:052105
- 23. Nayfeh AH (1981) Introduction to perturbation techniques. Wiley, New York
- 24. Kumar K, Tuckerman LS (1994) Parametric instability of the interface between two fluids. J Fluid Mech 279:49-68
- 25. Chandrasekhar S (1981) Hydrodynamic and hydromagnetic stability. Dover, New York
- Börzsönyi T, Tóth-Katona T, Buka A, Gránásy L (1999) Dendrites regularized by spatially homogeneous time-periodic forcing. Phys Rev Lett 83:2853

Publisher's Note Springer Nature remains neutral with regard to jurisdictional claims in published maps and institutional affiliations.

